Results in Physics 12 (2019) 1915–1924

Contents lists available at ScienceDirect

Results in Physics

journal homepage: www.elsevier.com/locate/rinp

Synthesis of a Cr-Cu surface alloy using a low-energy high-current electron beam

Alexey Markov[a,*], Evgenii Yakovlev[a,b], Daria Shepel'[a,b], Massimiliano Bestetti[c]

[a] Tomsk Scientific Center SB RAS, 10/4, Akademicheskii Pr., Tomsk 634055, Russia
[b] Institute of High Current Electronics SB RAS, 2/3, Akademicheskii Pr., Tomsk 634055, Russia
[c] Department of Chemistry, Materials and Chemical Engineering "Giulio Natta", Politecnico di Milano, Via Mancinelli 7, 20131 Milan, Italy

ARTICLE INFO

Keywords:
Surface alloy
Cr-Cu alloy
Pulsed electron beam
Wear resistance
Nanostructuring

ABSTRACT

A Cr-Cu surface alloy is synthesized using successive operations of Cr film deposition followed by mixing in a melted phase with the Cu substrate by a low-energy, high-current electron beam (LEHCEB). The parameters of LEHCEB are as follows: electron energy 20–30 keV and pulse duration 2–4 μs. Depending on the LEHCEB energy density, the concentration of Cr in the alloy is in the range from 60 to 20 at.%. The alloy microstructure has been analyzed, and its morphology is shown to represent nanosized chromium particles measuring 10–30 nm uniformly distributed in the copper matrix. The synthesized Cr-Cu surface alloys demonstrate a more than a factor of 3 a decrease in wear coefficient, which is nearly as low as the wear coefficient of Cr coatings. Some defects such as networks of cracks and pores, are observed in the lengthy regions of chromium. They are attributed to the tensile thermal stresses taking place during solidified melt cooling due to a large difference between the thermal expansion coefficients of copper and chromium.

Introduction

A Cr-Cu alloy is a basic material for producing electrodes for high-current vacuum interrupters operating at medium voltages. It is well known that the high electrical and thermal conductivity of copper-chromium alloys is ensured by their Cu matrix, and the Cr particles embedded into it improve the alloy wear resistance, contact erosion, and prevent the contacting surfaces from welding. A common method utilized for the production of such alloys is the powder metallurgy (PM) process involving uniaxial compaction of Cu and Cr powders, followed by their sintering. The quality of vacuum-electrical components manufactured by this method is, however, far from being perfect, which is mostly due to two major limitations — pores and oxygen present in the material, with Cu and Cr oxides formed due to the latter. That is why the density of the resulting Cr-Cu alloy is at best as high as 95% of the density of a cast material [1].

During manufacture, it is not so easy to achieve efficient service characteristics, since they depend on the material properties controlled not only by the concentrations of the components, Cr and Cu, but also by the alloy microstructure, specifically, by the grain size, their distribution, and morphology. For instance, it is known that chromium grain refinement improves the properties of the Cu–Cr contact material [2,3]. One of the methods that allow changing, in a wide range, both the microstructure of a material and its grain size is surface modification consisting of the pulsed power impact on metallic surfaces. The formation of a Cr-Cu alloy under non-equilibrium conditions of surface modification processes is appealing not only from a practical point of view but also in terms of fundamental investigations of the Cr-Cu system. The point is that in this system characterized by low mutual solubility of the elements under conditions of high-rate ($\sim 10^5$–10^9 K/s) melt quenching, we might expect an excessive solubility of the components and a formation of metastable phases with attractive properties. It is one more feature, which convinces to use the surface modification for the formation of alloys.

One of the surface modification methods, referred to as laser surface alloying (LSA), is quite common, e.g., in alloying of Cu [4,5]. During alloying, pure alloying dopants, such as Cr, W, Ni, Al or Ti, mixed with 4 wt% of a polyvinyl alcohol binder were applied onto Cu substrates using a brush, followed by the surface scanning with a 2 mm continuous laser beam [6,7]. After the Cr particles melted with the Cu matrix, the surface layer hardness increased, and the reaction rate of electro-mechanical erosion decreased, which according to the authors thinking was due to the formation of an oversaturated copper solution. It is worth mentioning that there are other literature data available on the possible formation of chromium – oversaturated copper solutions [8,9]. The limitation of the LSA method is its inability to form surface layers of

* Corresponding author.
E-mail address: almar@lve.hcei.tsc.ru (A. Markov).

https://doi.org/10.1016/j.rinp.2019.02.010
Received 2 November 2018; Received in revised form 25 January 2019; Accepted 4 February 2019
Available online 10 February 2019

Table 1
Surface alloy formation modes.

Mode	Charge voltage, kV	LEHCEB energy density, J/cm^2	Thickness of Cr film deposited per cycle, μm	Number of cycles	Number of irradiation pulses
1	22	4.6	0.1	10	10
2	25	5.7	0.1	10	10
3	27	6.3	0.1	10	10
4	30	7.0	0.1	10	10

defined chemical composition.

A surface layer with a defined chemical composition can be formed using some other surface modification processes – laser- or electron-beam cladding, where the powder is fed onto the surface of the substrate melted by the irradiation with a scanning laser- or electron beam and is fused into it [10,11]. Using a continuous scanning electron beam, a Cr-Cu surface layer was formed by *A. Schneider* and *V. Durakov* [12,13]. The size of Cr grains formed as a result of cladding (3–5 μm) was found to be much smaller than that formed by the PM process (50–100 μm). This decrease in the grain size resulted in better stability of cathode spot burning and lower chopping current. A disadvantage of this process consists in the necessity of subsequent mechanical finishing.

In the recent decade, a wide-aperture low-energy high-current electron beam (LEHCEB) of a microsecond duration has been successfully used for surface modification; in particular, it is installed as the main part of RITM-SP electron-beam machines (EBMs) [14,15]. An EBM is used for modification of metallic materials, for instance, pure titanium, nickel, zirconium, copper, and various steels and alloys [16–21]. In addition to surface irradiation, EBMs have become quite common in surface alloying or formation of surface alloys [22–26]. The formation of high-adhesion coatings – surface alloys, is an attractive method for improving the properties of components and parts. In a number of cases, in order to substantially improve the service properties, it is sufficient to form a defined elemental composition in the surface layer of a part, which is only a few micrometers (2–5) thick [15].

As far as the Cr-Cu alloys are concerned, so far LEHCEBs have been used for irradiation of surfaces of alloys prepared by standard processes, such as PM, in which the size of Cr inclusions was tens or even hundreds of micrometers [27–30]. The aim of such a treatment was formulated as both a technological task of cleaning from inclusions and smoothing electrode surfaces, as far as refining of recrystallized Cr grains, resulting in higher breakdown electrical fields of vacuum gaps, and a fundamental task of forming metastable phases and an attempt to solve the excessive fraction of Cr in Cu or Cu in Cr. One of the recent studies on modification of Cu with LEHCEBs deals with its alloying by tungsten; prior to irradiation W was applied to its surface in a powder form, similar to the LSA process [31].

The purpose of this work is to synthesize a Cr-Cu alloy immediately on a Cu substrate rather than merely irradiate the surface of a PM alloy. This was achieved by multiple depositions of thin Cr films and their intermixing in a liquid phase using LEHCEBs without breaking the vacuum. In addition, a study of morphology along with chemical and phase compositions of the synthesized surface alloy has been carried out, and its properties are compared with those of Cr-Cu alloys synthesized by other methods.

Experimental procedure

In this study the surface alloys were formed using a wide-aperture (beam diameter 80–100 mm) LEHCEB located in the same chamber with a number of magnetron sputtering systems, which allowed depositing films, melting them, and mixing in a liquid phase with the substrate in a single vacuum cycle. Technologically this approach was implemented in a RITM-SP EBM (Institute of High Current Electronics, OOO Microsplav) with the following parameters: electron energy of 10–30 keV, electron beam pulse duration of 2–4 μs, electron beam energy density on the target of 2–8 J/cm^2, film deposition rate of ~10 μm/h [14,15].

A Cr-Cu surface alloy was formed by alternating the operations of Cr film deposition on a Cu substrate, followed by subsequent irradiation of the resulting film/substrate system with a LEHCEB in a single vacuum cycle. The specimens (substrates) measuring 15 × 15 × 2 mm were manufactured from oxygen-free copper of the M00b grade (99.997 wt %). The surface roughness of the initial specimens R_a was of 1 ± 0.25 μm. Before film deposition, copper specimens were irradiated with a LEHCEB in order to clean and homogenize the surface. Optimal electron energy in this operation was determined experimentally and was found to be 25 keV. The films were deposited by magnetron sputtering from chromium of the ERCr-1 grade (99.95 wt%) at the deposition rate of 8.1 ± 0.2 μm/h. A 100 nm thick film was formed within one operation, the total number of deposition/irradiation cycles was 10, and thus the total thickness of the film deposited in the course of surface alloy formation was 1 μm. The modes of surface alloy formation are listed in Table 1. For a comparative analysis of the resulting surface alloy properties, we prepared a reference sample – a 1-μm chromium film deposited onto a copper substrate by a common magnetron sputtering process without LEHCEB irradiation.

A study of the surface layer morphology was conducted using optical and scanning electron microscopy (OM and SEM) in the MMU-3 (Russia), Philips SEM-515 (the Netherlands), and FEI Quanta 200 3D (the USA) electron microscopes. The surface topography was examined using the method of optical profilometry in an MNP-1 (Russia) and atomic-force microscopy (AFM) in a Solver HV (Russia) device. A chemical analysis of the surface was performed by the method of energy dispersive X-ray spectroscopy (EDS) at the accelerating voltage of 15 kV, which allowed analyzing a thin subsurface layer ~1 μm. The distribution of the elements over the depth of the specimens with the surface alloy was examined using Auger electron spectroscopy (Shkhuna − 2, Russia) and optical-emission spectroscopy in a glow discharge (Spectruma, Germany). A study of the phase composition of the specimens was carried out using the X-ray diffraction analysis in a Shimadzu XRD 6000 (Japan) diffractometer in a grazing incidence diffraction geometry at the incident angle of $\omega = 5^\circ$. An investigation of the microstructure was performed by the method of transmission electron microscopy (TEM) in a JEOL JEM2100 (Japan) electron microscope. The tribological tests were performed in a pin-on-disc mode in a TRIBOtester device (France). The counter body was a 3 mm ball made of Steel 100Cr6. The load on the specimen was 2 N, the sliding distance was 40 m, the track radius R was 2 mm, and the sliding velocity − 25 mm/s. The tests were performed under normal conditions without lubrication. The wear coefficient was calculated as$K_w = V_w/F_n a$, where V_w is the wear track volume; F_n – is the load on the specimen, and a – is the sliding distance. In the experiments with an optical profilometer, we determined S, the cross-section of wear track averaged over ten measurements made at different parts of the track. Then multiplying the averaged cross-section of the wear track S by track length $2\pi R$, the wear track volume V_w was obtained.

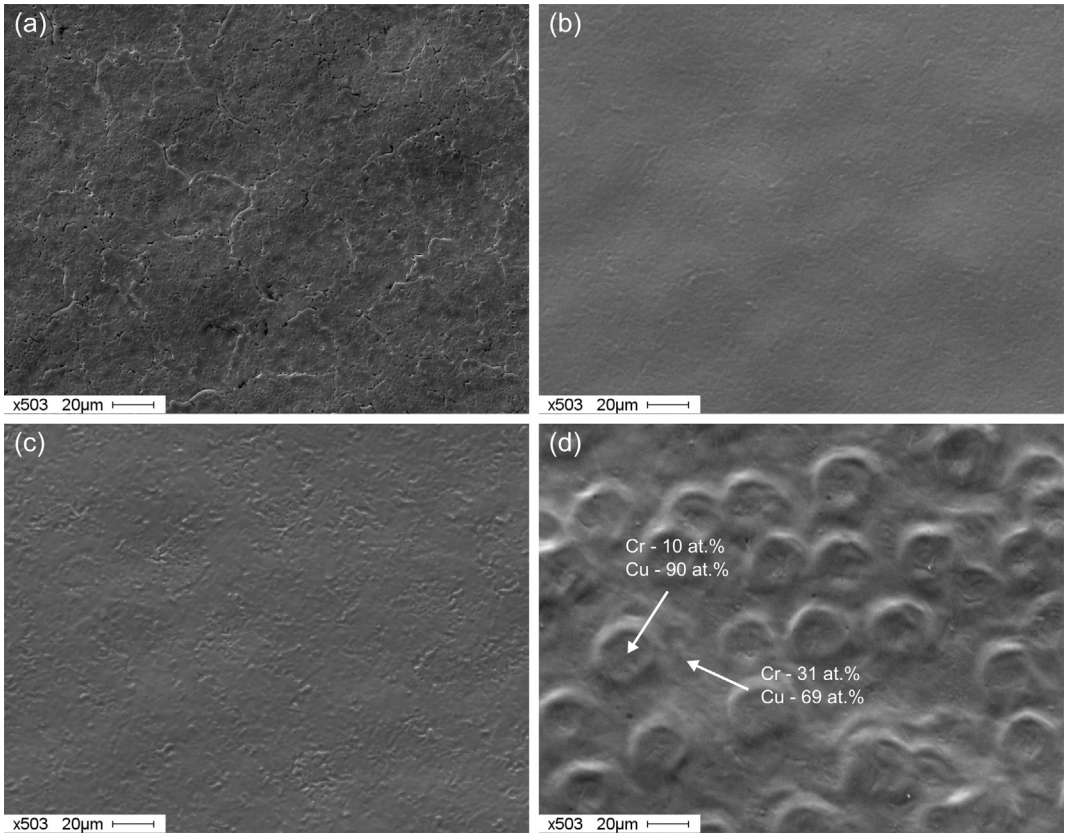

Fig. 1. SEM images of the specimen surfaces with a Cr-Cu alloy formed at the LEHCEB energy densities 4.6 (a), 5.7 (b), 6.3 (c) and 7.0 (d) J/cm$^{2.}$

Results

Figs. 1 and 2 present SEM images from the surfaces with the Cr-Cu surface alloy formed at different LEHCEB energy densities and the respective element distributions of Cr and Cu. An examination of the surface morphology demonstrated that depending on the LEHCEB energy density the surface relief patterns are noticeably different. Specifically, there are defects of the pore type on the entire surface of the Cr-Cu specimen, where the surface alloy was formed at the LEHCEB energy density of 4.6 J/cm^2 (Fig. 1a). This surface pattern implies the presence of non-homogeneous structure, high concentration gradients associated with incomplete mixing of the deposited chromium film with the copper substrate, which is consistent with the elemental analysis data (Fig. 2a). The surface roughness, in this case, was found to be 0.57 ± 0.1 μm. More effective mixing of the film and substrate materials is observed when the surface alloy is formed at the LEHCEB energy density of 5.7 J/cm^2 (Figs. 1b, 2b). In this case, the surface is smooth and free from defects; its roughness is 0.55 ± 0.1 μm. Similar results were obtained at the LEHCEB energy density of 6.3 J/cm^2 (Fig. 1c, 2c). When the LEHCEB energy density is, however, higher – 7 J/cm^2 (Fig. 1d, 2d), the elements begin to stratify and there are regions depleted in chromium, which measure 20–40 μm. The surface roughness in that mode was found to be 0.68 ± 0.1 μm. Thus, in terms of homogeneity of the Cr-Cu surface alloy, an optimal LEHCEB energy density is within the interval of 5.7–6.3 J/cm^2. It should be noted that only few craters were observed on the specimen surface with the Cr-Cu surface alloy irrespective of the LEHCEB energy density, which indicates high purity of the initial Cu.

Note that despite the smooth surface and absence of defects, even under optimal irradiation modes a noticeable scatter in the element concentrations throughout the surface can be observed in the images obtained by electron backscattering (EBS, see Fig. 3). It is evident that during surface alloy formation at the LEHCEB energy density of 5.7 J/cm^2, chromium particles measuring 1–5 μm begin to precipitate in the form of a dendrite-like structure (Fig. 3a), and the concentration of Cr across the surface is varied within the range from 30 to nearly 60 at.%. When the surface alloy is formed at the energy density of 6.3 J/cm^2 (Fig. 3b), the precipitation of fine individual Cr particles, whose size is ~1–2 μm, is observed.

Fig. 4 presents the research findings of the integral (from the area 100 × 100 μm^2) elemental composition of the specimens. During the EDS analysis, the electron energy was adjusted in such a way that the Cr concentration on the reference sample Cr(0.1)/Cu was 100% (see dotted line in Fig. 4). It is also evident in Fig. 4 that the concentrations of Cr and Cu on the surfaces of the specimens with the Cr-Cu surface alloy formed at energy density of 4.6 J/cm^2 are 59.7 and 40.3 at.%, respectively. When the LEHCEB energy density is increased, the concentration of Cr on the specimen surface decreases and Cu is increases that suggests a more intensive liquid-phase mixing of the film and substrate materials at high LEHCEB energy densities along with a formation of thicker regions of the Cr-Cu surface alloys. At the energy density of 7 J/cm^2, the concentrations of Cr and Cu in the surface layer sharply change and are found to be of 21.2 and 78.8 at. %, respectively. According to the EDS point analysis, the elemental composition on the oval convex regions, formed at this LEHCEB energy density, differs from that on the rest of the surface (Fig. 1d). It was identified that the average content of Cr in the center of the oval convex regions is 10 at. %, which is by more than three factors lower than for the rest of the surface, where the concentration of Cr is equal to 31 at.%. The mechanism of this elemental stratification is likely to be due to the liquid-phase segregation of the Cr-Cu alloys well known from the literature [5].

Fig. 5 presents the profiles of the element concentrations with respect to the depth of a 300 nm layer of the initial Cu specimens, of the LEHCEB-irradiated specimen, and the specimen with a Cr-Cu surface alloy formed at the LEHCEB energy density of 5.7 J/cm^2, obtained by

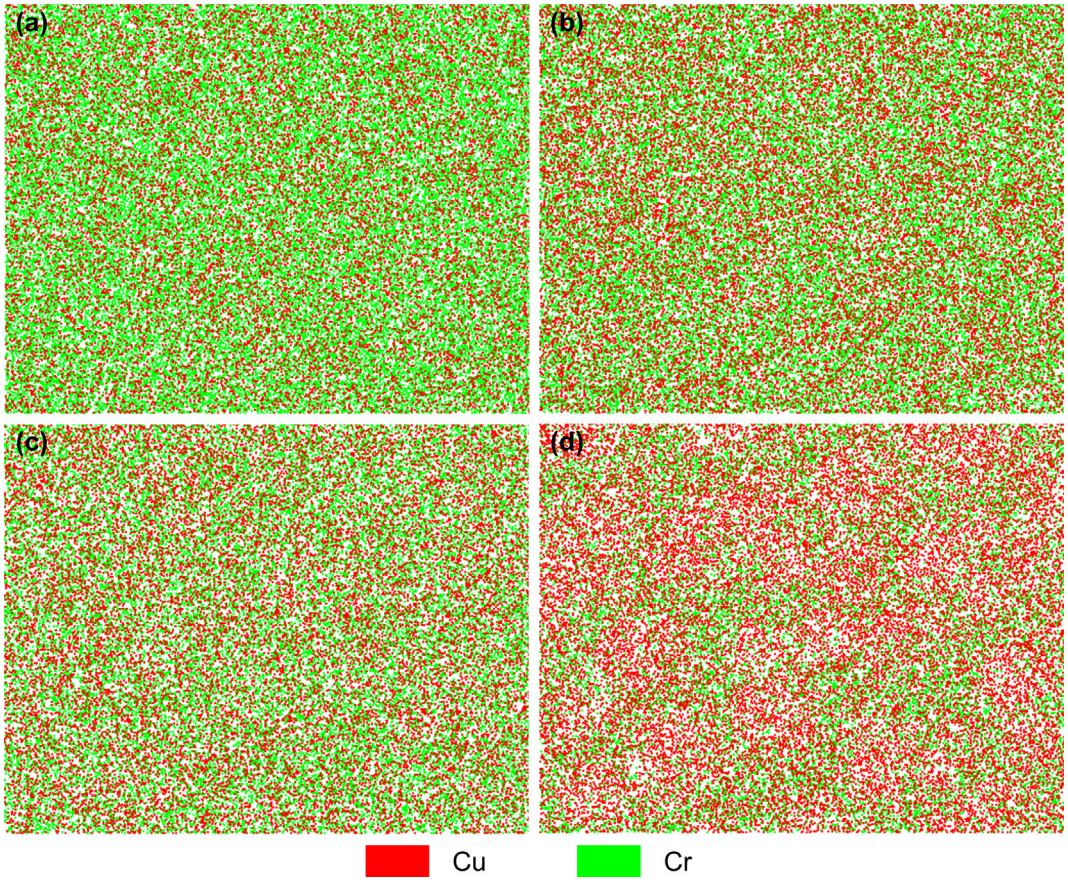

Fig. 2. Distribution of Cu and Cr across the specimen surfaces with the Cr-Cu surface alloys formed at different LEHCEB energy densities: 4.6 (a), 5.7 (b), 6.3 (c) and 7.0 (d) J/cm$^{2.}$

the Auger electron spectroscopy. It is evident that after the LEHCEB irradiation the subsurface layer of Cu is cleaned from the impurities of oxygen and, which is especially critical, carbon, whose concentration in a 100-nm subsurface layer of the initial specimen is quite high. While there are oxygen and carbon impurities in the resulting Cr-Cu surface alloy, the contaminated layer thickness is essentially smaller (~25 nm) than in the initial specimen (~100 nm). The distribution of Cr and Cu over the depth is quite homogeneous; their average concentrations are found to be of 28 and 69 at.%, respectively.

The element distributions over the depth for a 5 μm layer of the specimens with the surface alloy formed at different LEHCEB energy densities are presented in Fig. 6. It is clear that the Cr concentration at the LEHCEB energy density of 5.7 J/cm^2 has a sharp curve in the region of 1.7–1.8 μm, and at the LEHCEB energy density of 6.3 J/cm^2 this curve is more gradual and is found deeper in the specimen – at about 2 μm. This suggests alloying of copper with chromium at deeper subsurface layers as the LEHCEB energy increases. It is also evident from Fig. 6 that the concentration of Cr decreases as the LEHCEB energy density increases, which is consistent with the data obtained by the EDS method. Note also that areas under the Cr concentration curves are practically the same, which suggests that the deposited chromium does not virtually evaporate from the surface in the course of the surface alloy formation.

According to the calculations, the melted surface layer thickness is ~3 μm. Thus, an XRD analysis of the specimens with a Cr-Cu surface alloy in the grazing incidence geometry (analyzed depth ~2 μm) provides the data on the melted layer only [32]. The results of the phase composition investigations on the specimens with a Cr-Cu surface alloy are presented in Fig. 7 in comparison with the reference and initial Cu specimens. It is clear that the initial Cu specimen consists of an FCC-copper with the lattice parameter $a = 3.6157$ Å. The reference specimen, in addition, consists of BCC-chromium with the lattice parameter $a = 2.9042$ Å, both phase lattice parameters agree with the tabulated data. The formation of a Cr-Cu surface alloy does not change the phase composition, changing the phase ratio only. For instance, for the specimen with a Cr-Cu surface alloy formed at the LEHCEB energy density of 4.6 J/cm^2 the copper and chromium phase contents are 61 and 39%, respectively. An increase in the LEHCEB energy density results in a smaller fraction of the Cr phase and, hence, a larger fraction of the Cu phase; at the energy density of 7 J/cm^2 they constitute 7 and 93%, respectively. After the surface alloy is formed, there is a slight shift of the lines towards a larger angle. It suggests emerging tensile microstresses formed as a result of rapid melt quenching.

During the formation of a Cr-Cu surface alloy, the specimen surfaces undergo nanostructuring. Fig. 8 presents the surface topography images obtained by the atomic-force microscopy for different LEHCEB energy densities. The grain sizes for the specimens with a Cr-Cu layer formed at the energy densities of 4.6 and 5.7 J/cm^2 are found to be 50–100 nm, and at the LEHCEB energies 6.3 and 7 J/cm^2 they are 25–50 nm, respectively.

Fig. 9 presents the images of the microstructure formed in the subsurface layer of the specimen with a Cr-Cu surface alloy formed at the LEHCEB energy density of 5.7 J/cm^2, microdiffraction patterns, and dark-field images formed in the respective reflections obtained by the TEM method. It is clear that the structure of the resulting surface layer has nanoparticles (Fig. 9a), whose microdiffraction represents a combination of point and ring structures (Fig. 9b); the latter pattern is typical for nanocrystalline materials. An interpretation of the microdiffraction pattern allowed identifying that the main phase is that of copper with comparatively large grains measuring 200–500 nm (Fig. 9d), and the ring diffraction, corresponding to nanosized particles, belongs to the Cr-phase. The Cr particles are evenly distributed

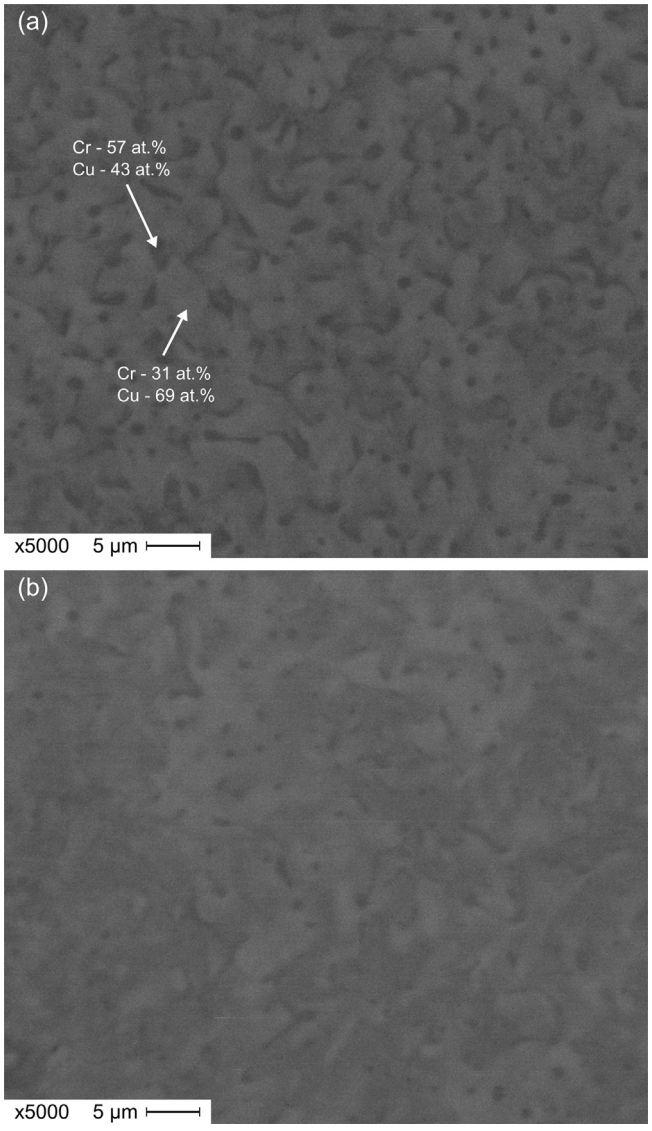

Fig. 3. EBS images of the specimen surfaces with the Cr-Cu surface alloys formed at the LEHCEB energy densities 5.7 (a) and 6.3 (b) J/cm$^{2.}$

throughout the entire region under study and their sizes lie within 10–30 nm (Fig. 9a, b). This finding is a quite important, since such a nanostructure has not been observed in the investigation of Cr-Cu alloys modified by LEHCEBs. The minimal size was commonly no less than 1 μm; in our case, the ultrafine Cr precipitates are by nearly two orders of magnitude smaller.

The results of tribological testing of the specimens with a Cr-Cu surface alloy in comparison with those for the reference, pure Cu, and commercially produced $Cr_{30}Cu_{70}$ (wt.%) alloy sintered by PM method (size of embedded Cr particles ~10 μm) specimens are presented in Fig. 10. According to the data presented, the wear coefficient of the initial Cu specimen is 3.06×10^{-4} mm^3/(N × m). The wear coefficient of the reference specimen (a 1-μm chromium film deposited onto a copper substrate) is essentially – more than a factor of 4, lower (0.72×10^{-5} mm^3/(N × m)), which is to be expected; this is accounted for by high hardness and tribological characteristics of Cr coatings [33]. Unfortunately, such low wear coefficient values are unattainable for the specimens with Cr-Cu surface alloys, since the presence of 'soft' copper reduces their wear resistance. Nevertheless, the minimum wear coefficient demonstrated by the specimen with a Cr-Cu surface layer formed at the LEHCEB energy density of 4.6 J/cm^2 (0.98×10^{-5} mm^3/(N × m)) was close to that of the reference specimen. Its value is three

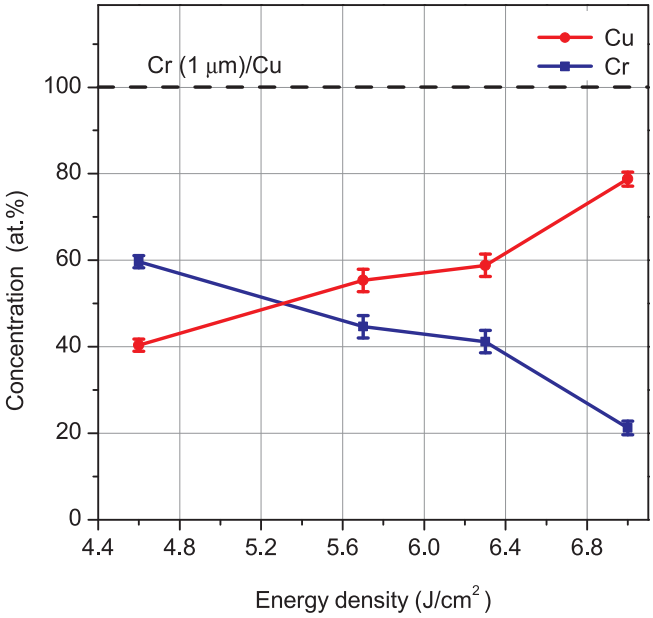

Fig. 4. Integral elemental composition of the specimen surfaces with the Cr-Cu surface alloy as a function of the LEHCEB energy density.

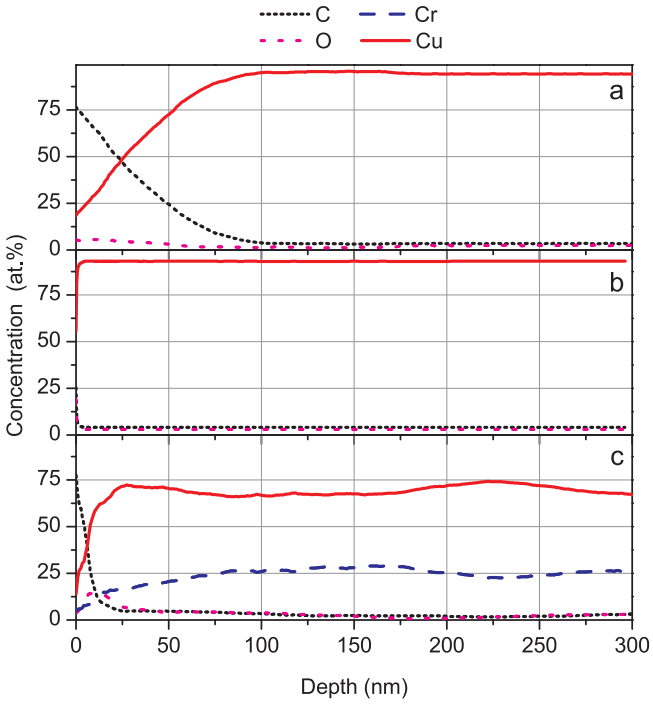

Fig. 5. Element distribution over the specimen depth obtained by the Auger method for the initial specimen (a), specimen irradiated with LEHCEB (b), and specimen with a Cr-Cu alloy formed at the LEHCEB energy density 5.7 J/cm^2 (c).

times less that of the initial specimens. As the LEHCEB energy density increases (and hence the concentration of Cr in the subsurface layer decreases), the specimen wear resistance drops. For instance, at the LEHCEB energy density of 7.0 J/cm^2 the wear coefficient is found to be 2.61×10^4 mm^3/(N × m), which is only 15% lower than that of the initial Cu specimen. However, under the optimal modes of formation of Cr-Cu surface alloys the specimen wear coefficient is by 30–35% lower than that of the initial specimen, which could be considered as a good result.

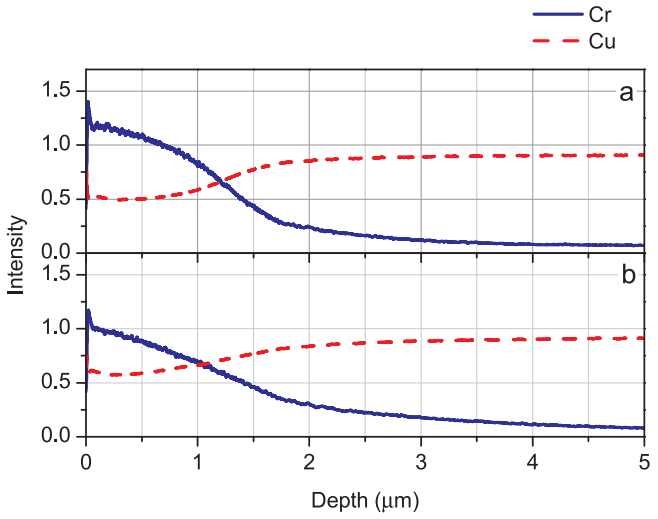

Fig. 6. Element distribution over the specimen depth obtained by the GDOES method from the Cr-Cu surface alloy formed at the LEHCEB energy densities 5.7 (a) and 6.3 (b) J/cm^2.

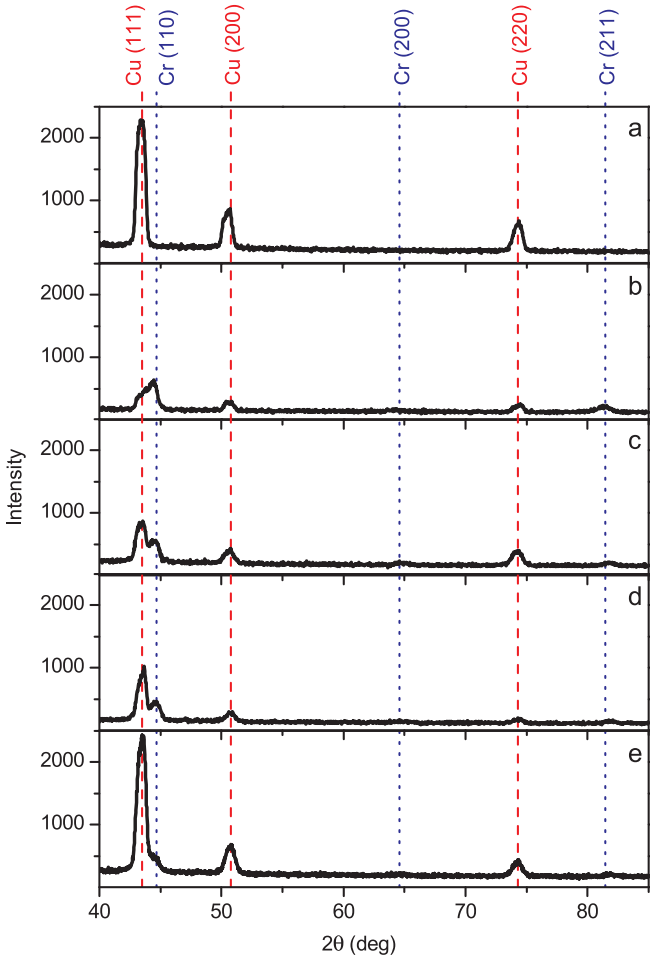

Fig. 7. XRD patterns obtained in the grazing incidence geometry. Initial Cu specimen (a), Cr(0.1)/Cu reference specimen (b) and specimens with the surface alloys formed at 4.6, 5.7, and 7.0 J/cm^2 (c, d, e), respectively.

Discussions

Oversaturated solid solution

The issue of the formation of a Cr-Cu oversaturated solid solution under non-equilibrium conditions is not only a theoretical challenge, but it is also of practical interest as well. This interest stems from the fact that dispersion-hardened copper alloys could be manufactured using an oversaturated Cr-Cu solid solution. In this study, despite super-high velocities of melt cooling, we did not observe any formation of a Cr-Cu oversaturated solid solution: the analytic methods demonstrated the formation of a Cr and Cu two-phase mixture, where the concentration of the solved elements corresponded to an equilibrium state diagram. Other studies [27–29] dealing with modification of the Cr-Cu alloy by LEHCEBs report some contradicting data.

For instance, in [27] the authors reported a LEHCEB irradiation of a $Cu_{70}Cr_{30}$ (wt.%) alloy. Using the data obtained by the focused ion beam – secondary-ion mass spectroscopy, they revealed a simultaneous presence of both Cr and Cu in certain areas of Cr grains irradiated with a LEHCEB, relying on which they announced synthesis of a non-equilibrium Cr-Cu compound, which they also termed a solid solution. It should be recalled that this compound was formed only under irradiation of the specimens by high-energy-density LEHCEBs, while no mutual mixing of these elements occurred under specimen irradiation at low energy densities, the interfaces between Cu and Cr remained distinct. The authors however did not report any direct validation of that synthesis by the XRD or TEM data.

An assumption was made in [28,29], where the authors irradiated $Cu_{75}Cr_{25}$ and $Cu_{50}Cr_{50}$ (wt.%) alloys with LEHCEBs and analyzed them afterwards, that no oversaturated solid solution was formed in [27] – it was merely an ordinary mixture of two phases. The latter conclusion is supported by the fact that an XRD examination of the specimens irradiated by LEHCEBs using the similar mode did not reveal any new phases in addition to the initial Cu and Cr. On the other hand, the surface morphology after irradiation changes cardinally: between the initial Cr and Cu grains there appear evenly distributed Cr spheroids measuring ~1 μm, which is essentially smaller than the initial Cr grain size. It is likely that it was the structure morphology, which provided in [27] the pattern of the presence of two elements in the same local spatial region, relying on which the authors made a conclusion on the formation of an oversaturated solid solution.

The data that we report here, validating the constancy of phase composition of the surface layer after irradiation with LEHCEBs, agree with those reported elsewhere [28,29]. Despite the seeming difference in the conditions of the liquid-phase mixing used in these works, they are quite similar. In one case, liquid Cr and Cu intermix along the beam incidence (film-substrate system), while in the other case they are intermixed in the direction normal to the beam incidence (PM specimens). Note that in both cases however, due to a large difference in the thermal properties of these elements, their mixing occurs under conditions of high temperature gradients, i.e., it is intensified by micro-capillary convection. During fast heating, a homogeneous Cr-Cu melt forms, while in the course of its fast cooling a liquid-phase separation of the elements takes place, resulting in precipitation of Cr in the form of finely dispersed phase crystallizing afterwards, which is followed by crystallization of Cu having a lower melting temperature.

Thus, one of the principal conclusions concerning the aforementioned studies – the constancy of the phase composition of a surface layer irradiated with LEHCEB: even considerably non-equilibrium conditions do not allow fixing new metastable phases. This seems to be due to very short times of the melt persistence – liquid copper sustains for a few microseconds, and liquid chromium – less than 1 μs, due to its high melting temperature. The latter could be seen in Fig. 11 where the temporal dependence of the melt thickness for the case of irradiation of the Cr(0.1)/Cu system with LEHCEB at the energy density of 6.3 J/cm^2 is presented [32]. Lifetimes of the melted Cu and Cr are 1.9 and 0.2 μs,

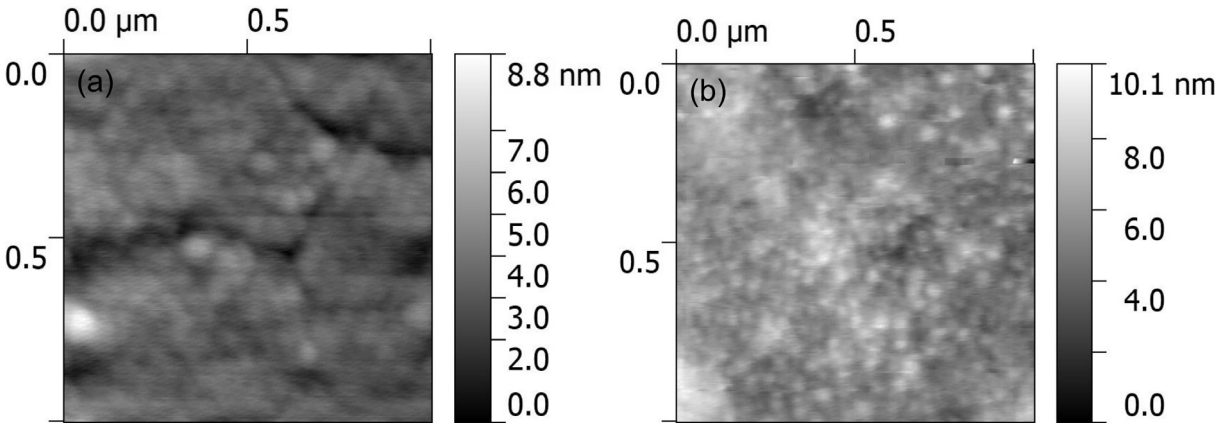

Fig. 8. Images of the specimen topography with the Cr-Cu surface alloys formed at the LEHCEB energy densities 4.6 (a) and 6.3 (b) J/cm$^{2.}$

respectively. So, the mutual melt of a film (Cr) and substrate (Cu) persists for ~0.2 μs only followed by their fast crystallization. The maximum melt thickness is 3.2 μm, and the average rate of the melt crystallization is 15.5 m/s. Knowing the lifetime of Cr melt and the size of Cr particles, we can estimate roughly the rate of Cr particle growth which is ~0.1 m/s.

Interestingly, in the case where a contact material is irradiated with a 4.5 mm cw laser beam at the specimen scanning velocity of 3.5–8 mm/s, and the melt persistence time is noticeably longer than in the case of LEHCEB, the authors argue that in the remelting and subsequent recrystallization zone they observed an oversaturated solution of Cu in Cr, the concentration of the former achieving ≈10 at.% [9]. It is to be noted that in addition to Cu and Cr the initial powder material contained 4 wt.% Fe. The authors of [34,35] reported the presence of chromium particles with a large content of copper, e.g., $Cr_{88}Cu_{12}$ particles during arc-discharge mel ting and superfast melt quenching. The

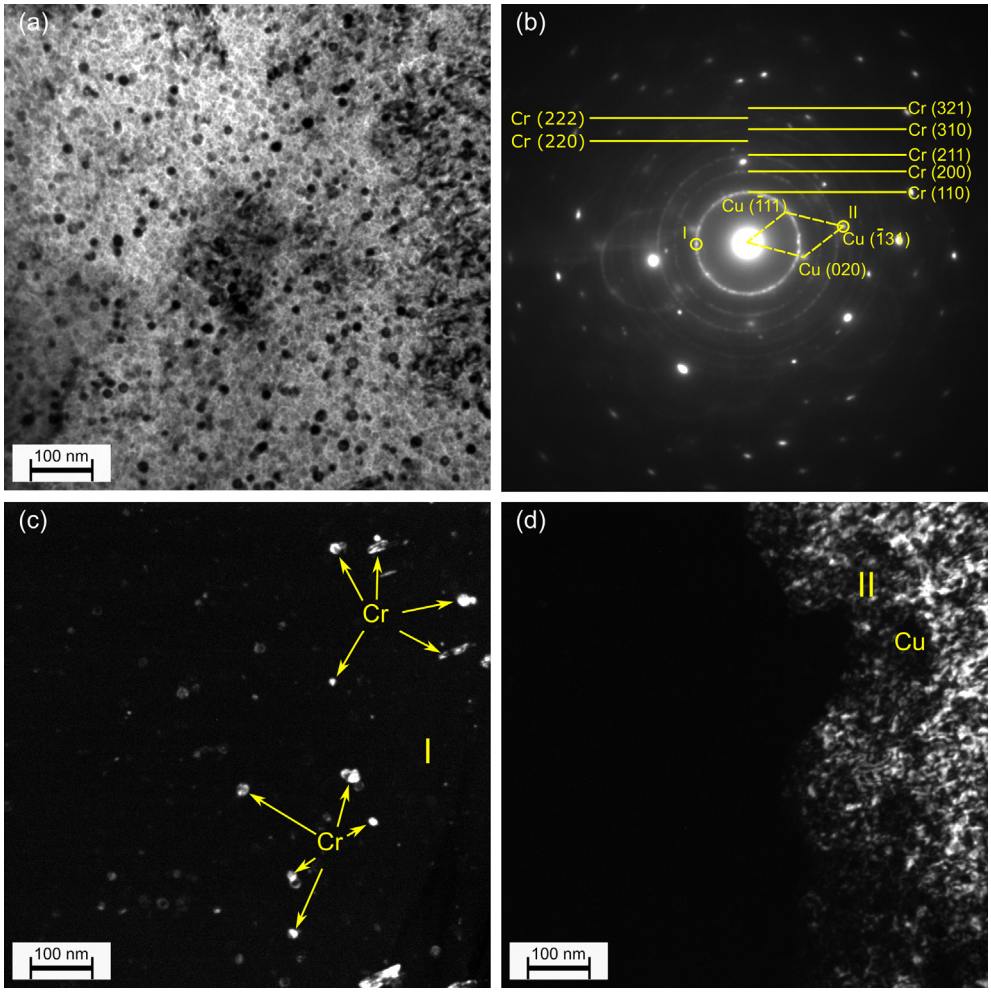

Fig. 9. TEM images of the subsurface layer of the specimen with a Cr-Cu surface alloy formed at the LEHCEB energy density 5.7 J/cm^2: a – bright-field image, b – microdiffraction pattern, c – dark-field image obtained in the reflection of the first diffraction ring denoted I, and d – dark-filed image obtained in the reflection from Cu denoted II.

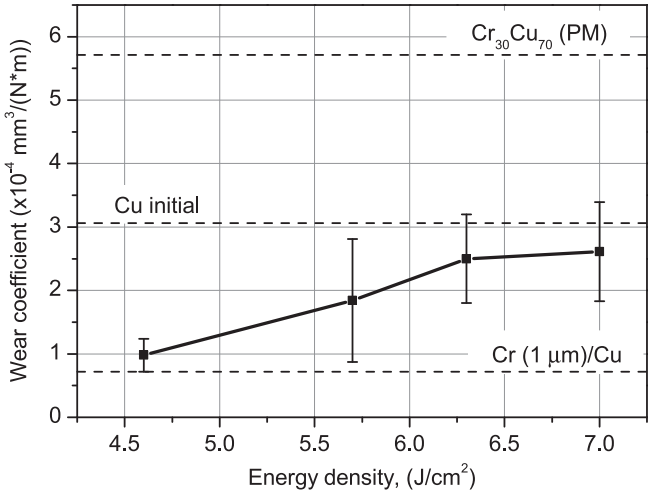

Fig. 10. Wear coefficients of the specimens with Cr-Cu surface alloys as a function of the LEHCEB energy density.

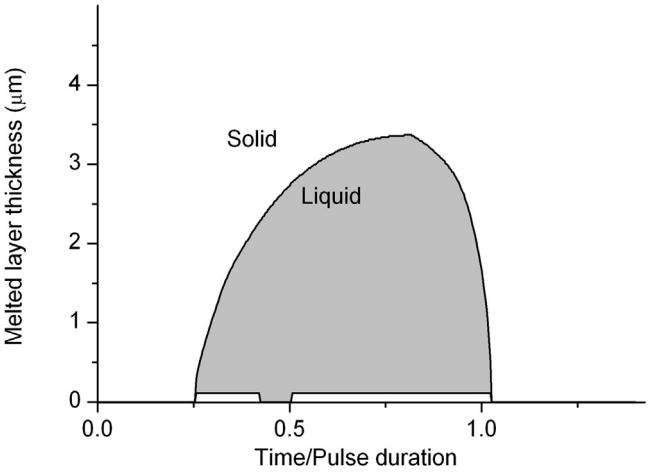

Fig. 11. Temporal dependence of the melt thickness for the case of irradiation of the Cr(0.1)/Cu system with LEHCEB at the energy densities 6.3 J/cm^2.

presence of oversaturated chromium and copper solutions was revealed by the EDS analysis. Had we limited ourselves by the EDS analysis only and did not performed TEM, then, relying on the EDS data, we could have arrived at the same conclusion about the formation of oversaturated solutions of chromium and copper, see Figs. 3 and 4. A more precise TEM analysis, however, demonstrates that during superfast cooling a large number of evenly distributed nanosized Cr particles are formed in the copper matrix, in other words, the structure whose investigation by such integral methods as EDS might create an illusion of formation of solid solutions of a non-equilibrium composition.

Surface defects

The most valuable information on the surface state after its LEHCEB irradiation or synthesis of surface alloys is that on its topography, in particular, such defects as craters. Craters can deteriorate the surface properties of materials, and their formation is commonly undesirable. The formation of craters is a factor preventing an extensive use of LEHCEBs in industrial applications.

After irradiation of a Cr-Cu alloy specimen manufactured by the PM process, craters and cracks were observed on its surface [28,29]. All cracks were found in Cr grains, while the craters were predominantly located either at the Cr grain junctions or even at the cracks. The authors report that in the $Cu_{75}Cr_{25}$ and $Cu_{50}Cr_{50}$ (wt.%) they did not

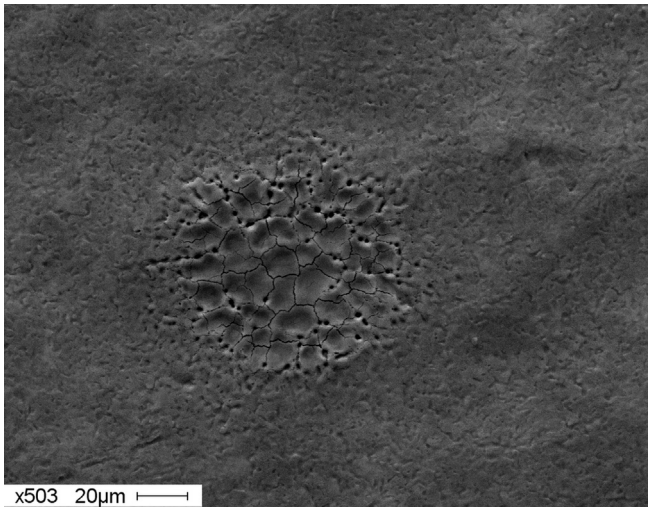

Fig. 12. SEM images of the surface with the Cr-Cu alloy formed at the LEHCEB energy density 5.7 J/cm^2.

observe any second-phase inclusions in either copper or chromium and that craters are formed on the vacancy clusters or voids rather than on Cu and Cr inclusions, as it was demonstrated in steel or titanium alloys [36]. The formation of cracks was attributed to quasi-static pressures and low plasticity of Cr.

In our case, the situation with defects is quite similar to that described in the above-mentioned studies [27,28]. There are nevertheless certain differences. In particular, there are no initial Cr grains in our case, since the surface alloy is synthesized on a copper substrate as a result of liquid-phase mixing by a LEHCEB. Yet, in the course of the synthesis, we observed lengthy chromium regions not mixed with the copper substrate. For instance, Fig. 12 shows such a region measuring approximately 50 μm. The concentration of Cr in its center, obtained by the EDS method, is 95 at. %, i.e., it is a layer of pure chromium about 1 μm in thickness. A network of cracks and a large number of pores have been revealed. In this case it is reasonable to refer to these defects as pores rather than craters, since there are no features of a classical crater, such as large transverse dimensions measuring tens or even hundreds of microns and a characteristic axis-symmetrical shape with a microhole in the center. The dimensions of pores in our case are found to be 1–5 μm, in many cases their contours are non-symmetrical. It is evident in Fig. 12 that most pores are located on the cracks and some of them – on double or triple joints of the cracks. The situation observed here reminds the process of a spalling crack formation under the action of high-power relativistic electron beams (REBs) on metals. Only in the case of REBs, a wave of tensile stresses gives rise to the formation of micropores, followed by a subsequent nucleation of microcracks, while in our case the process is reverse: first microcracks nucleate and then pores are formed on them [37].

The dynamics of the surface layer formation allows identifying the mechanism by which cracks are formed in Cr grains. During crystallization of the surface melt, chromium particles are the first to crystallize, since the crystallization temperature of chromium is nearly 800 K higher than that of copper. Copper is the second to crystallize, and then the copper matrix and the embedded chromium particles together undergo fast cooling. During cooling the linear dimensions of the metal decrease. It should be recalled that chromium is a metal with a low thermal expansion coefficient (TEC), while the TEC of copper is by 2–3 factors higher. Thus, during cooling a particle of Cr would be affected by tensile stresses from the copper matrix. The value of these stresses can be estimated using the formula

$$\sigma = E\Delta\alpha\Delta T,$$

where E – is the Young modulus, $\Delta\alpha$ – is the difference between TECs of

chromium and copper, and ΔT – is the difference between the crystallization and room temperatures.

The estimations performed by this formula yield σ = 2–3 GPa, which is a few times higher than the ultimate tensile strength of chromium. Thus, it is evident that it is the tensile stresses operating during cooling which cause cracking. A large number of pulses used in LEHCEB irradiation give rise to thermal cycling, during which both the number of cracks and their size are rising, which eventually results in a network of cracks presented in Fig. 12.

Wear resistance

As for the tribological testing results, one can state that all the specimens with Cr-Cu surface alloy have a higher wear coefficient than a reference specimen (a 1-μm chromium film deposited onto a copper substrate). Taking into account the above and comparing Figs. 4 and 10, it becomes clear that the wear coefficient of the sample only indirectly depends on the energy density of LEHCEB. In fact, it is determined by the concentration of chromium in the surface layer, and the latter is higher, the lower the wear coefficient. One can expect this result because Cr is one of the hardest and most wear resistant metals. Therefore, it is evident that the maximum wear resistance among all used irradiation modes for Cr-Cu surface alloy can be observed just for the LEHCEB energy density of 4.6 J/cm^2 when the chromium concentration is the highest and constitutes 60 at. %.

However, the role of the nanocrystalline microstructure, which is realized during the formation of Cr-Cu surface alloy (see. Fig. 9), is equally important in terms of a wear resistance increase. It becomes clear when we compare the wear coefficient of commercially produced $Cr_{30}Cu_{70}$ (wt.%) alloy sintered by a PM method and Cr-Cu surface alloy synthesized by LEHCEB with close Cr concentrations given in Fig. 10. The first is more than two times higher than the second. Moreover, it is even higher than the wear coefficient for pure Cu. At first sight, a high value of wear coefficient for commercially produced $Cr_{30}Cu_{70}$ (wt.%) alloy sintered by the PM method is unclear because the addition of a very high wear resistant element Cr into the Cu matrix has to enhance the wear resistance of the alloy. It can be explained by the fact that the friction conditions for Cr-Cu alloy are quite different from those for pure Cu and Cr (a reference specimen). Indeed, for pure Cu we have soft Cu material and soft Cu debris appearing in the friction process. For pure Cr, we have hard Cr material and hard Cr debris. As for sintered $Cr_{30}Cu_{70}$ (wt.%) alloy, we have two kinds of debris – soft Cu and hard Cr. These hard particles of Cr probably cause the enhanced Cu removal from the friction zone between a steel ball and Cr-Cu surface during the friction with soft Cu material. Since the size of nanocrystalline chromium particles in LEHCEB synthesized Cr-Cu surface alloy is substantially smaller than the particle size of chromium in $Cr_{30}Cu_{70}$ (wt.%) alloy sintered by PM, different friction conditions and different wear pattern are provided for these two types of alloys. The only reasonable explanation is that during the friction process of Cr-Cu surface alloy synthesized by LEHCEB, the hard Cr debris does not appear or it is too small to substantially remove Cu from the friction zone between the steel ball and Cr-Cu surface.

Thus, the combination of a high concentration of chromium and a formed nanocrystalline microstructure for a specimen irradiated with LEHCEB energy density of 4.6 4.6 J/cm^2 ensures a low wear coefficient.

Conclusions

A Cr-Cu surface alloy has been synthesized immediately on the Cu substrate, with the Cr concentration varying from 60 to 20 at.%, depending on the LEHCEB energy density. An optimal mode of the LEHCEB energy density, at which the resulting alloy is sufficiently homogeneous and the surface defects are few, has been determined. It has been demonstrated that at lower LEHCEB energy densities the elements do not completely mix and the surface contains such defects as pores and cracks. At higher LEHCEB energy density Cr and Cu have been observed to separate due to the liquid-phase segregation of the Cr-Cu surface alloy.

Despite the non-equilibrium conditions of formation of the Cr-Cu surface alloy under superfast cooling, the phase composition of the resulting surface alloy is consistent with the equilibrium state diagram. The morphology of the alloy is extraordinary: it represents nanosized chromium particles measuring 10–30 nm, which are uniformly distributed in the copper matrix.

Under some of the LEHCEB modes investigated in this study, the wear coefficient of the synthesized Cr-Cu surface alloys is reduced more than a factor of 3 compared with that of the initial Cu specimens and nearly as low as that of Cr coatings.

Following the formation of the Cr-Cu surface alloy, the lengthy regions consisting of chromium have been observed to contain defects – networks of cracks and a large number of pores. The reasons for these defects are the tensile thermal stresses generated during cooling of the melt due to a large difference between the thermal expansion coefficients of copper and chromium.

References

[1] Papillon A, Roure S, Schellekens H, Missiaen JM, Chaix JM, Rigal E. Investigation on the chemical reactions affecting the sinterability and oxide content of Cu–Cr composites during the solid state sintering process. Mater Des 2017;113:353–60. https://doi.org/10.1016/j.matdes.2016.09.038.

[2] Slade Paul G. The vacuum interrupter: theory, design and application. CRC Press; 2007.

[3] Rieder WF, Schussek M, Glatzle W, Kny E. The influence of composition and Cr particle size of Cu/Cr contacts on chopping current, contact resistance, and breakdown voltage in vacuum interrupters. IEEE Trans Components, Hybrids, Manuf Technol 1989;12:273–83. https://doi.org/10.1109/33.31434.

[4] vonAllmen M, Blatter A. Melting and solidification BT – laser-beam interactions with materials: physical principles and applications. In: von Allmen M, Blatter A, editors, Berlin, Heidelberg: Springer Berlin Heidelberg; 1995. p. 68–114. https://doi.org/10.1007/978-3-642-57813-7_4.

[5] Majumdar JD, Manna I. Introduction to laser assisted fabrication of materials. In: Majumdar JD, Manna I, editors, Laser-assisted Fabr. mater. Berlin, Heidelberg: Springer Berlin Heidelberg; 2013. p. 1–67. https://doi.org10.1007/978-3-642-28359-8_1.

[6] Wong PK, Kwok CT, Man HC, Cheng FT. Laser surface alloying (LSA) of copper for electrical erosion resistance. In: Kwok C, editor, Laser surf. modif. alloy. corros. eros. resist., WOODHEAD PUBL LTD; 2012. p. 288–319. https://doi.org/10.1016/B978-0-85709-015-7.50008-7.

[7] Kwok CT, Wong PK, Man HC. Laser surface alloying of copper with titanium: Part I. Electrical wear resistance in dry condition. Part II. Electrical wear resistance in wet and corrosive condition. Surf Coatings Technol 2016;297:58–73. https://doi.org/10.1016/j.surfcoat.2016.04.008.

[8] Kostrubiec F, Pawlak R, Walczak M. Laser modification of properties of the surface layer of conducting materials. Proc. SPIE – Int. Soc. Opt. Eng. 2003. p. 197–205. https://doi.org/10.1117/12.520717.

[9] Geng H-R, Liu Y, Chen C-Z, Sun M-H, Gao Y-Q. Laser surface remelting of Cu-Cr-Fe contact material. Mater Sci Technol 2000;16:564–7. https://doi.org/10.1179/026708300101508081.

[10] Węglowski MS, Błacha S, Phillips A. Electron beam welding – techniques and trends – review. Vacuum 2016;130:72–92. https://doi.org/10.1016/j.vacuum.2016.05.004.

[11] Morimoto J, Abe N, Kuriyama F, Tomie M. Formation of a Cr_3C_2/Ni-Cr alloy layer by an electron beam cladding method and evaluation of the layer properties. Vacuum 2001;62:203–10. https://doi.org/10.1016/S0042-207X(00)00439-5.

[12] Schneider A, Popov S, Durakov VG, Dampilon BV, Dehonova SZ, Batrakov A. On breaking capacity of the $CuCr_{25}$ composite material produced with electron-beam cladding. Proc. – int. symp. discharges electr. insul. vacuum, ISDEIV 2012. p. 269–71. https://doi.org/10.1109/DEIV.2012.6412505.

[13] Durakov VG, Dampilon BV, Gnyusov SF. Properties and features of structure formation CuCr-contact alloys in electron beam cladding. AIP conf. proc. 2014. p. 135–8. https://doi.org/10.1063/1.4898901.

[14] Markov AB, Mikov AV, Ozur GE, Padei AG. A РИТМ-СП facility for the surface alloying. Instruments Exp Tech 2011;54:862–6. https://doi.org/10.1134/S0020441211050149.

[15] Markov AB, Yakovlev EV, Petrov VI. Formation of surface alloys with a low-energy high-current electron beam for improving high-voltage hold-off of copper electrodes. IEEE Trans Plasma Sci 2013;41:2177–82. https://doi.org/10.1109/TPS.2013.2254501.

[16] Zhang XD, Hao SZ, Li XN, Dong C, Grosdidier T. Surface modification of pure titanium by pulsed electron beam. Appl Surf Sci 2011;257:5899–902. https://doi.org/10.1016/j.apsusc.2011.01.136.

[17] Zhang C, Zhang Y, Tian N, Chen S, Qian Z, Lv P, et al. Microstructures of pure nickel induced by high-current pulsed electron beam irradiation. Prot Met Phys Chem

Surfaces 2016;52:869–75. https://doi.org/10.1134/S2070205116050269.
[18] Chai L, Chen B, Wang S, Zhang Z, Murty KL. Microstructural, textural and hardness evolution of commercially pure Zr surface-treated by high current pulsed electron beam. Appl Surf Sci 2016;390:430–4. https://doi.org/10.1016/j.apsusc.2016.08.128.
[19] Zhang K, Ma J, Zou J, Liu Y. Surface microstructure and property modifications in a duplex stainless steel induced by high current pulsed electron beam treatments. J Alloys Compd 2017;707:178–83. https://doi.org/10.1016/j.jallcom.2017.01.003.
[20] Liu YR, Zhang KM, Zou JX, Liu DK, Zhang TC. Effect of the high current pulsed electron beam treatment on the surface microstructure and corrosion resistance of a Mg-4Sm alloy. J Alloys Compd 2018;741:65–75. https://doi.org/10.1016/j.jallcom.2017.12.227.
[21] Zhang Z, Yang S, Lv P, Li Y, Wang X, Hou X, et al. The microstructures and corrosion properties of polycrystalline copper induced by high-current pulsed electron beam. Appl Surf Sci 2014;294:9–14. https://doi.org/10.1016/j.apsusc.2013.12.178.
[22] Meisner LL, Markov AB, Rotshtein VP, Ozur GE, Meisner SN, Yakovlev EV, et al. Microstructural characterization of Ti-Ta-based surface alloy fabricated on TiNi SMA by additive pulsed electron-beam melting of film/substrate system. J Alloys Compd 2018;730:376–85. https://doi.org/10.1016/j.jallcom.2017.09.238.
[23] Zhang C, Lv P, Cai J, Zhang Y, Xia H, Guan Q. Enhanced corrosion property of W-Al coatings fabricated on aluminum using surface alloying under high-current pulsed electron beam. J Alloys Compd 2017;723:258–65. https://doi.org/10.1016/j.jallcom.2017.06.189.
[24] Tang G, Luo D, Tang S, Mu Q, Wang L, Ma X. The microstructure and properties of Cr alloying layer after surface alloying treatment induced by high current pulsed electron beam. J Alloys Compd 2017;714:96–103. https://doi.org/10.1016/j.jallcom.2017.04.014.
[25] Luo D, Tang G, Ma X, Gu L, Wang L, Wu T, et al. The microstructure of Ta alloying layer on M50 steel after surface alloying treatment induced by high current pulsed electron beam. Vacuum 2017;136:121–8. https://doi.org/10.1016/j.vacuum.2016.11.036.
[26] Xia H, Zhang C, Lv P, Cai J, Jin Y, Guan Q. Surface alloying of aluminum with molybdenum by high-current pulsed electron beam. Nucl Instrum Methods Phys Res Sect B Beam Interact Mater Atoms 2018;416:9–15. https://doi.org/10.1016/j.nimb.2017.11.028.
[27] Lamperti A, Ossi PM, Rotshtein VP. Surface analytical chemical imaging and morphology of Cu-Cr alloy. Surf Coatings Technol 2006;200:6373–7. https://doi.org/10.1016/j.surfcoat.2005.11.103.
[28] Zhou ZM, Chai LJ, Xiao ZP, Tu J, Wang YP, Huang WJ. Surface modification of Cu-25Cr alloy induced by high current pulsed electron beam. Trans Nonferrous Met Soc China (English Ed) 2015;25:1935–43. https://doi.org/10.1016/S1003-6326(15)63801-8.
[29] Chai LJ, Zhou ZM, Xiao ZP, Tu J, Wang YP, Huang WJ. Evolution of surface microstructure of Cu-50Cr alloy treated by high current pulsed electron beam. Sci China Technol Sci 2015;58:462–9. https://doi.org/10.1007/s11431-015-5774-7.
[30] Dong S, Zhang C, Zhang L, Cai J, Lv P, Jin Y, et al. Microstructure and properties of Cu-Cr powder metallurgical alloy induced by high-current pulsed electron beam. J Alloys Compd 2018;755:251–6. https://doi.org/10.1016/j.jallcom.2018.04.291.
[31] Zhang C, Lv P, Cai J, Peng CT, Jin Y, Guan Q. The microstructure and properties of tungsten alloying layer on copper by high-current pulse electron beam. Appl Surf Sci 2017;422:582–90. https://doi.org/10.1016/j.apsusc.2017.06.049.
[32] Rotshtein V, Ivanov Y, Markov A. Surface treatment of materials with low-energy, high-current electron beams. In: Mater. surf. process. by dir. energy tech., Elsevier; 2006. p. 205–40. https://doi.org/10.1016/B978-008044496-3/50007-1.
[33] Daure JL, Carrington MJ, Shipway PH, McCartney DG, Stewart DA. A comparison of the galling wear behaviour of PVD Cr and electroplated hard Cr thin films. Surf Coatings Technol 2018. https://doi.org/10.1016/J.SURFCOAT.2018.06.070.
[34] Wei X, Wang J, Yang Z, Sun Z, Yu D, Song X, et al. Liquid phase separation of Cu-Cr alloys during the vacuum breakdown. J Alloys Compd 2011;509:7116–20. https://doi.org/10.1016/j.jallcom.2011.04.017.
[35] Sun ZB, Wang YH, Guo J. Liquid phase separation of Cu-Cr alloys during rapid cooling. Trans Nonferrous Met Soc China (English Ed) 2006;16:998–1002. https://doi.org/10.1016/S1003-6326(06)60367-1.
[36] Zou J, Zhang K, Dong C, Qin Y, Hao S, Grosdidier T. Selective surface purification via crater eruption under pulsed electron beam irradiation. Appl Phys Lett 2006;89. https://doi.org/10.1063/1.2234306.
[37] Dudarev EF, Markov AB, Mayer AE, Bakach GP, Tabachenko AN, Kashin OA, et al. Spall fracture patterns for the heterophase Cu-Al-Ni alloy in ultrafine- and coarse-grained states exposed to a nanosecond relativistic high-current electron beam. Russ Phys J 2013;55:1451–7. https://doi.org/10.1007/s11182-013-9979-6.